ACS APPLIED MATERIALS & INTERFACES

Research Article

www.acsami.org

Exploring High Refractive Index Silicon-Rich Nitride Films by Low-Temperature Inductively Coupled Plasma Chemical Vapor Deposition and Applications for Integrated Waveguides

Doris K. T. Ng,*[,†] Qian Wang,[†] Ting Wang,[‡] Siu-Kit Ng,[†] Yeow-Teck Toh,[†] Kim-Peng Lim,[†] Yi Yang,[†] and Dawn T. H. Tan[‡]

[†]Data Storage Institute (A*STAR) Agency for Science Technology & Research, DSI Building, 5 Engineering Drive 1, Singapore 117608, Singapore

[‡]Photonics Devices and Systems Group, Singapore University of Technology and Design, 8 Somapah Road, Singapore 487372, Singapore

ABSTRACT: Silicon-rich nitride films are developed and explored using an inductively coupled plasma chemical vapor deposition system at low temperature of 250 °C with an ammonia-free gas chemistry. The refractive index of the developed silicon-rich nitride films can increase from 2.2 to 3.08 at 1550 nm wavelength while retaining a near-zero extinction coefficient when the amount of silane increases. Energy dispersive spectrum analysis gives the silicon to nitrogen ratio in the films. Atomic force microscopy shows a very smooth surface, with a surface roughness root-mean-square of 0.27 nm over a 3 μm × 3 μm area of the 300 nm thick film with a refractive index of 3.08. As an application example, the 300 nm thick silicon-rich nitride film is then patterned by electron beam lithography and etched using inductively coupled plasma system to form thin-film micro/nano waveguides, and the waveguide loss is characterized.

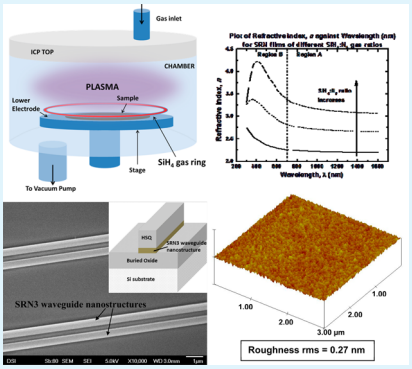

KEYWORDS: *silicon-rich nitride, SRN, ICP-CVD, refractive index, waveguides, nonlinear optics, CMOS compatible*

1. INTRODUCTION

Research into silicon (Si) as a photonic material has seen significant progress in recent years. Because of its compatibility with complementary metal oxide semiconductor (CMOS) processing, low optical absorption at the telecommunications wavelength, and large linear and nonlinear refractive index, Si-based waveguide devices have been demonstrated for a plethora of applications.[1−5] Si however has drawbacks as a nonlinear material, as a result of its small, indirect band gap at 1550 nm[6] wavelength. Consequently, within a waveguide with high mode confinement, the onset of nonlinear losses occurs even at low powers of hundreds of milliwatts when continuous wave light is used.

Another material of interest is silicon nitride (SiN_x). SiN_x is a centrosymmetric, CMOS compatible material shown to be useful for integrated optics[7] and possesses interesting nonlinear properties.[8−11] There is also the absence of two-photon absorption and free carrier effects at the telecommunications wavelength as compared to Si.

Focusing on the benefits of both Si and SiN_x, we explore another type of CMOS compatible material with great potential as a nonlinear material,[12] silicon-rich nitride (SRN). As SRN gives a refractive index that can be tailored between SiN_x and Si, we deposit a range of films using low-temperature inductively coupled plasma chemical vapor deposition (ICP-CVD). SRN films are explored with the purpose of overcoming the issue of nonlinear losses at 1550 nm wavelength while still being CMOS compatible. It has also attracted significant attention very recently in the areas of solar cell for efficiency improvement[13,14] and integrated photonics[7,15] as a waveguide material.[12] When used as a waveguide material, SRN has the capability of high-density device integration (submicrometer waveguide cross-section with a strong light confinement) similar to Si material, while simultaneously facilitating applications in nonlinear optics across a wider wavelength range as compared to Si due to the ability to engineer a larger band gap. In addition, with the right process conditions, SRN can be made to possess a high nonlinear refractive index, while also having low linear and nonlinear losses such as two-photon absorption and free carrier effects at the telecommunications wavelength as compared to Si. These characteristics make it an attractive material for nonlinear photonics.

SRN films are commonly grown by plasma enhanced chemical vapor deposition (PECVD)[16] at a temperature of 300−500 °C or low-pressure chemical vapor deposition (LPCVD)[17] at a temperature of ∼800 °C. When LPCVD is used, the films will be required to be annealed at 1100 °C to reduce the number of N−H bonds in the film and out-diffuse the hydrogen as the presence of N−H bonds can have deleterious effects on optical components. Specifically, N−H

Received: July 14, 2015
Accepted: September 16, 2015
Published: September 16, 2015

DOI: 10.1021/acsami.5b06329
ACS Appl. Mater. Interfaces 2015, 7, 21884−21889

bonds act as absorption centers, and their low energy tail leads to undesirable absorption loss in the region of 1510−1565 nm.[18,19] As an alternative to these two common deposition methods for Si-rich films, we explore the SRN deposition using ICP-CVD. ICP-CVD is a technique that enables high-quality films to be grown at process temperatures as low as 250 °C. The deposited SRN films by ICP-CVD are characterized and analyzed, and SRN integrated ultrathin film waveguides are demonstrated as an application example.

Section 2 gives the details of material growth, characterization, and film analysis. ICP-CVD is a one-step direct growth of SRN (without the need for any postgrown annealing process[20]) at a relatively low temperature of 250 °C using an ammonia-free gas chemistry of $SiH_4/N_2/Ar$. The use of N_2 instead of NH_3 during the deposition process will reduce the overall amount of H in the gas chemistry and hence reduces the overall presence of N−H bonds, which will act as absorption centers. The SRN films deposited under different deposition conditions are characterized via a spectro-ellipsometer for the refractive index and extinction coefficient, and via an energy dispersive spectrum (EDS) for the material composition. Analysis results show that we are able to tailor the film's refractive index (n) from 2.2 to 3.08 measured at 1550 nm wavelength with a near-zero extinction coefficient through controlling the SiH_4/N_2 ratio.

As an example, the 300 nm thick SRN film with a refractive index of 3.08 (at 1550 nm) is chosen for ultrathin film waveguide demonstration in section 3. Surface roughness measurements of this film show an ultrasmooth surface roughness root-mean-square (RMS) of 0.27 nm over a 3 μm × 3 μm area. The films were patterned using electron beam lithography (EBL) and etched by inductively coupled plasma (ICP), which gives a ∼90° sidewall profile. The integrated ultrathin film 4 μm wide waveguide is characterized through Hakki-Paoli optical loss measurement,[21] which gives a propagation loss of 7.5 dB/cm.

2. SRN FILMS DEPOSITION BY ICP-CVD AND CHARACTERIZATIONS

SRN Deposition by ICP-CVD. ICP-CVD growth is achieved by using a plasma in which the gases react in a flow discharge. This discharge ionizes the gases, creating active species that react at the wafer surface. The ICP-CVD has a high-density-plasma source (ICP source) in which the plasma electrons are excited in a direction parallel to the chamber boundaries, by a magnetic potential set up by a coil wound outside dielectric walls. Figure 1 shows a schematic of the ICP-CVD chamber configuration (Oxford Instruments PlasmaPro System 100). There is a silane (SiH_4) gas ring directly above the sample stage to bring the SiH_4 gas nearer to the substrate. An ammonia-free gas chemistry of $SiH_4/N_2/Ar$ with gas flows controlled by electronic mass flow controllers was explored. The process chamber is a hybrid configuration consisting of an ICP source and a radio frequency (RF) powered wafer chuck. Helium backside cooling of the wafer is used for efficient heat transfer.

In this work, 300 nm thick SRN films were deposited on 4 μm thick silica on a Si substrate at a temperature of 250 °C, which is much lower as compared to growth by PECVD[16] and LPCVD.[17] The ICP source power was kept at 2000 W, and the pressure was set at 25 mTorr. The process started with conditioning the chamber by running the SRN recipe for 10 min with just a Si carrier plate in the chamber. This will coat a thin layer of SRN on the chamber wall and set the chamber in SRN deposition ambient. Ideally, prior to SRN chamber conditioning, the chamber should have a layer of SiO_2 on its wall. This will ensure better adhesion of the SRN film on the chamber wall, hence preventing flakes of SRN films from falling onto the sample during the deposition. For SRN deposition, the sample will be put on an 8-in. Si carrier and transferred by a loadlock arm into the process chamber. Once in the high vacuum process chamber, the sample will be soaked in Ar gas ambient for 5 min before the actual SRN deposition starts. This will ensure uniform heat distribution throughout the sample during deposition. Three samples are prepared during the deposition, and the corresponding deposition conditions for these three samples are summarized in Table 1. A major tuning factor in the deposition for these three samples is the SiH_4/N_2 ratio, which is 0.85, 1.36, and 2.27, respectively, for these three samples, SRN1, SRN2, and SRN3. This ratio will affect the film composition and refractive index accordingly as shown in the following. The RF power also differs among the three depositions, which affects the film deposition rate and has some influence on the refractive index.

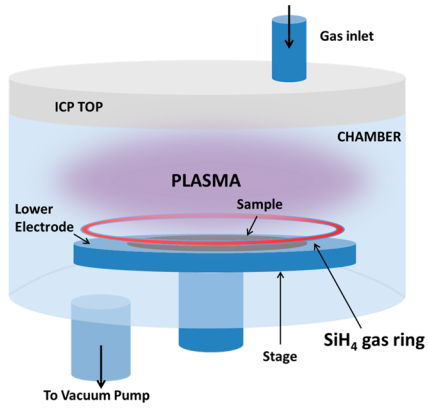

Figure 1. Schematic of the ICP-CVD (Oxford Instruments PlasmaPro System 100) system used to deposit the SRN films.

Characterization of SRN Films and Analysis. The deposited films were first characterized for their refractive indices and extinction coefficients (k) using the spectro-ellipsometer from wavelengths of 300−1600 nm. The obtained refractive indices and extinction coefficients for these three SRN films are shown in Figure 2a and b, respectively.

The plots show that as the SiH_4:N_2 gas flow ratio increases, the deposited film's refractive index increases for the entire range from 300 to 1600 nm. The same trend is observed for k from these films. However, beyond a wavelength of 700 nm, k from these films goes to 0. At a wavelength of 1550 nm, these three SRN films show n = 2.20 (SRN1), 2.66 (SRN2), and 3.08 (SRN3). Their SiH_4:N_2 gas flow ratios during deposition are 0.85 (SRN1), 1.36 (SRN2), and 2.27 (SRN3), respectively. All three films have k = 0 at 1550 nm wavelength. If there is no absorption in the material, the index will decrease toward longer wavelengths (region A of Figure 2). When absorption occurs, the index will be affected. If the absorption is strong, it will cause a change in direction for n, which will return to normal dispersion after the absorption drops back down. This region of strong absorption (region B of Figure 2) is referred to as anomalous dispersion. The energy bandgaps of these three films were also extracted during the ellipsometer measurement. Using the Cody−Lorentz[22] dispersion model for SRN fitting, the energy bandgaps show a decrease from 1.86 to 1.75 eV as

DOI: 10.1021/acsami.5b06329
ACS Appl. Mater. Interfaces 2015, 7, 21884−21889

Table 1. ICP-CVD Deposition Conditions for SRN Films SRN1, SRN2, and SRN3

	gas flow					power				
film ID	SiH_4 [sccm]	N_2 [sccm]	SiH_4/N_2 ratio	Ar [sccm]	pressure [mTorr]	ICP [W]	RF [W]	temp [°C]	He cooling [Torr]	deposition rate [nm/min]
SRN1	34	40	0.85	50	25	2000	2	250	5	24.5
SRN2	34	25	1.36	60	25	2000	10	250	5	14.0
SRN3	34	15	2.27	50	25	2000	20	250	5	8.3

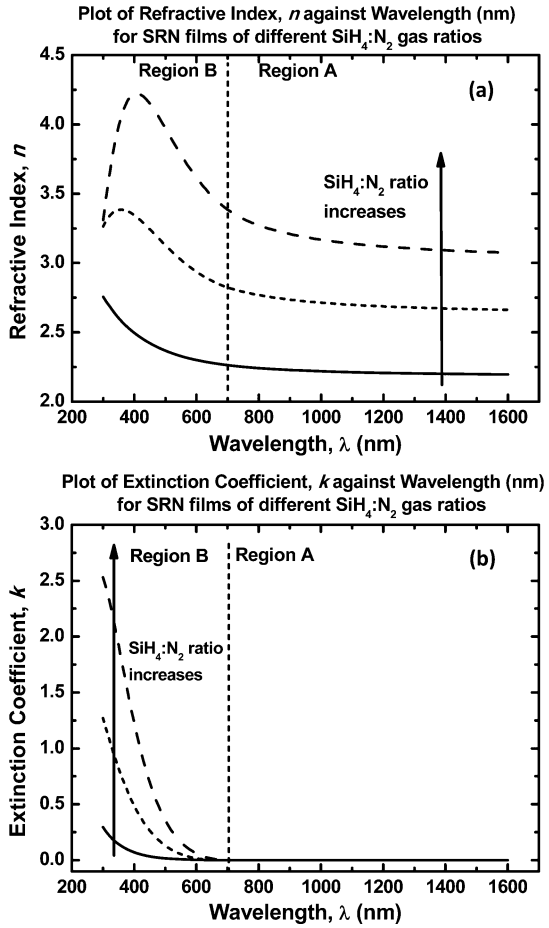

Figure 2. Ellipsometer measurements of SRN films of different SiH_4:N_2 gas flow ratios from 300 to 1600 nm wavelength range. The trend of (a) n and (b) k with wavelengths is observed.

the film's refractive index increases. This value is between that of SiN (5 eV) and Si (1.1 eV). Hence, refractive indices of SRN films can be tailored by precise control of the SiH_4:N_2 gas flow ratios, and they will subsequently affect the films' energy bandgaps. The refractive indices of these three films increase mainly due to the increase in the SiH_4:N_2 gas flow ratio during the deposition. Variation in the SiH_4:N_2 gas flow ratio will affect the films' refractive indices, while Ar acts as a buffered gas in the deposition process. The main reacting gases to form SRN in the deposition process are SiH_4 and N_2 as $SiH_4 + N_2 \rightarrow SiN_x + H_2$, which is different from the commonly used SiH_4 and NH_3 in PECVD. The replacement of NH_3 with N_2 will indicate less H in the film, hence possibly minimizing the presence of N−H bonds' absorption centers.

The main mechanism in increasing the film's refractive index lies in the amount of Si and N contents in the deposited film, which is further verified by analyzing two films using energy dispersive spectrum (EDS). Figure 3 shows the EDS obtained

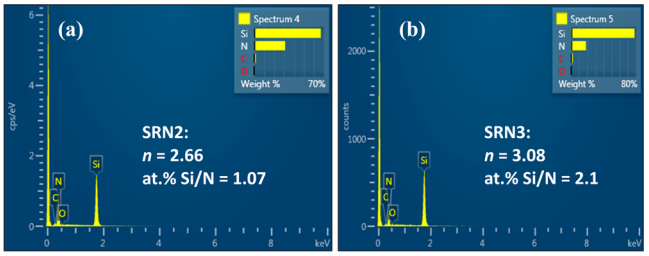

Figure 3. EDS showing the presence of Si and N in (a) SRN2 and (b) SRN3 films. The Si/N atomic % increases as the SRN film deposited becomes more Si-rich.

from SRN2 and SRN3. EDS shows the presence of Si and N in the films. C and O are in small amounts, common in EDS due to the carbon tape used for sticking the sample and some contaminants from sample handling. As the film's refractive index increases, the film's Si/N atomic % increases, which means that the film is getting more Si-rich (SRN3).

In our experiment, we also explore the influence of RF power during deposition. Figure 4 shows that a change in RF power

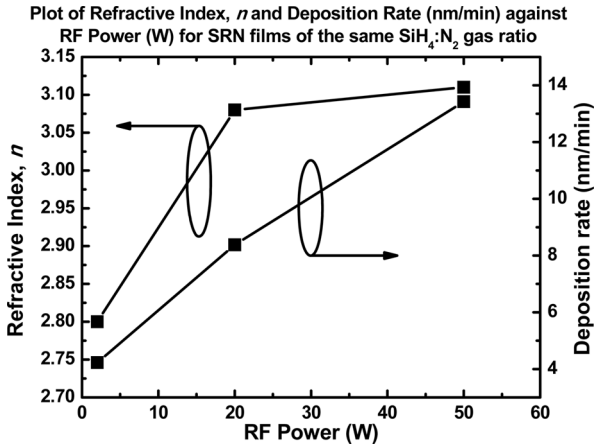

Figure 4. Graph showing refractive indices (n) and deposition rate of SRN films of the same SiH_4:N_2 gas flow ratio with respect to change in RF power. These results are within tolerance of $\pm 10^{-3}$.

will also change the film's refractive index and deposition rate. SRN films with the same SiH_4:N_2 gas flow ratio but different RF powers were deposited. The ellipsometer measurements show that as RF power increases, the films' refractive indices increase. This is because the RF power helps to attract the plasma generated at the ICP tube toward the film during deposition. The higher is the RF power, the faster will the plasma be attracted toward the substrate as the substrate is seated on top of the lower electrode where the RF power is. This faster attraction of plasma onto the substrate for a higher RF power also means denser plasma during deposition, hence a faster deposition rate and denser film with higher refractive

DOI: 10.1021/acsami.5b06329
ACS Appl. Mater. Interfaces 2015, 7, 21884−21889

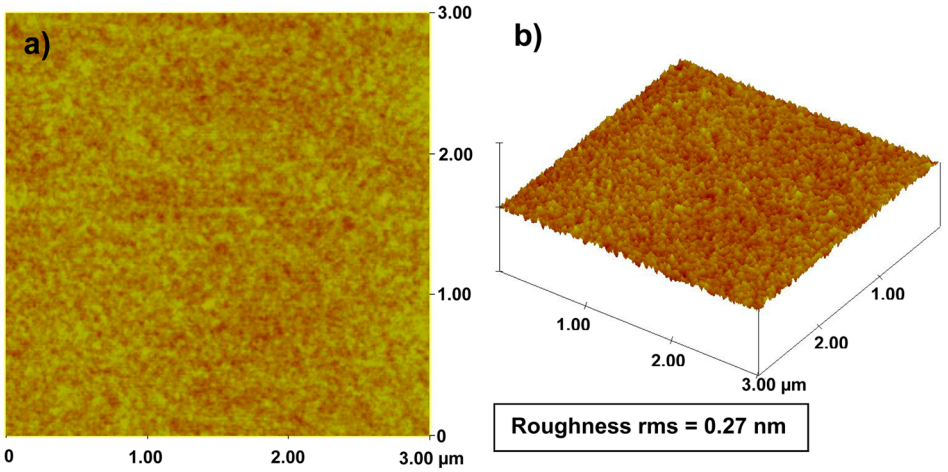

Figure 5. AFM images showing (a) two-dimensional and (b) three-dimensional scans over a 3 μm × 3 μm area of SRN3 film on Si substrate with 1 μm BOX. Vertical scale is 10 nm. Roughness rms is 0.27 nm.

index as RF power increases. A point to take note of is that too high an RF power might have detrimental effects on the film deposition, resulting in a rougher film or the substrate being etched away when the plasma gets too dense, moves too fast toward the substrate, and starts bombarding the substrate instead of depositing on the substrate.

3. DEMONSTRATION OF ULTRATHIN FILM WAVEGUIDE

The SRN film deposited with the highest n = 3.08 at wavelength 1550 nm (typical wavelength used in integrated photonics) was measured for its surface roughness using AFM. SRN film with the highest refractive index (SRN3) was chosen for further characterization and fabrication. The surface roughness of SRN3 was measured using tapping mode atomic force microscopy (AFM). Figure 5a and b shows the AFM scans of ∼300 nm thick SRN3 film deposited on Si substrate with 1 μm BOX. The root-mean-square (rms) surface roughness of SRN3 is 0.27 nm within a 3 μm × 3 μm scan area. This is comparable with the substrate roughness of 0.2 nm, that indicates an ultrasmooth surface, which will be one of the factors to ensure better material for propagation within the waveguides.

This film was then patterned by electron beam lithography (EBL) using hydrogen silsesquioxane (HSQ-FOX24) as the mask. HSQ was spun on SRN deposited on Si substrate with 1 μm BOX at a spin speed of 3000 rpm for 60 s. The sample was then soft baked at a temperature of 120 °C for 2 min, followed by 180 °C for 3 min. This was followed by a second coating of E-spacer (300z Ax-01) on the sample with a spin speed of 2000 rpm for 60 s. The sample was baked again at 95 °C for 1 min. Exposure was done at a dosage of 2000 μC/cm^2 at a current of 1 nA with chip size of 600 μm^2 and dot map of 240 000. After EBL exposure, the sample was developed using 25% TMAH for 30 s to define the pattern, rinsed with DI water, and blow dried with N_2. ICP dry etching using a gas chemistry of SF_6 and CHF_3 was used to transfer the pattern down to the SRN film. The chamber pressure was set at 15 mTorr with a gas mixture of SF_6 (9 sccm) and CHF_3 (50 sccm). ICP power was set at 1000 W with RF power at 33 W. Substrate temperature was kept at −20 °C. The etch rate observed was around 9 nm/s.

There are two types of waveguides included in the experiment, 4 μm wide waveguide and 450 nm wide waveguide. Figure 6a and b shows the SEM images of nanostructures fabricated using SRN3 film with EBL patterning followed by a

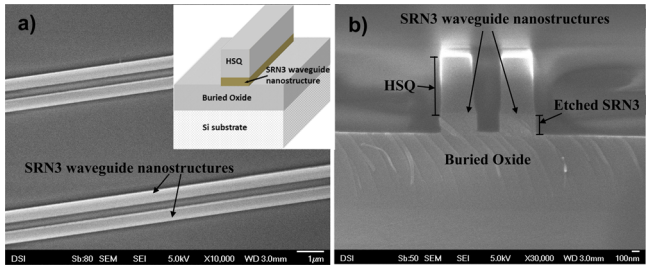

Figure 6. SEM images showing (a) top view and (b) cross-sectional view of SRN3 waveguide nanostructures fabricated. Inset shows schematic of SRN3 fabricated structure. Width of etched SRN feature is 450 nm.

SF_6 and CHF_3 ICP etching. Figure 6b shows an etched sidewall profile of ∼90° with an etched depth of ∼260 nm for a feature with a line width of 450 nm. The thickness of the HSQ mask etched is ∼30 nm. The selectivity of the HSQ mask to SRN3 etch measured in this work is around 1:8.7, which is considerably good as HSQ is an e-beam resist. An etched sidewall profile of ∼90° contributes to better mode confinement during waveguide propagation.

To better understand the different loss factors contributing to the overall propagation losses inherent in waveguides fabricated from our films, we fabricated waveguides with a width of 4 μm. The loss coefficients of the 4 μm wide waveguides were characterized using the Hakki−Paoli approach,[21] which measures the transmission of the Fabry−Perot response formed by the waveguide facets, combined with the overall transmission loss. The corresponding transmission is shown in Figure 7 when the input power is about 4.5 mW. The coupling efficiency between the input objective lens and front waveguide end is about 20%, and the coupling efficiency between the output objective lens and rear waveguide end is about 30%. The loss of the waveguide was estimated to be ∼7.5 dB/cm by taking account of this spectrum (peak-to-value ratio), facet reflectance (∼30%), and overall transmission loss. The 4 μm width implies that the extent of mode confinement within the waveguide is low. Therefore, the intensity of the E-field in contact with the sidewalls is minimal, and thus any

DOI: 10.1021/acsami.5b06329
ACS Appl. Mater. Interfaces 2015, 7, 21884−21889

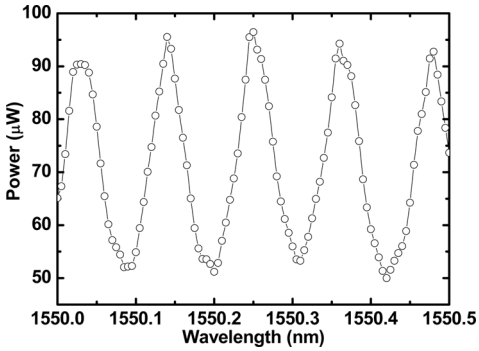

Figure 7. Transverse electric mode Fabry–Perot resonance of a 4 μm wide, 4 mm long SRN waveguide measured at telecommunications wavelength.

losses will be mainly dominated by the material losses. In this case, we would expect that the upper limit of the material losses from our SRN films is ~7.5 dB/cm. Another important aspect for SRN waveguide is its nonlinear property and application in all-optical signal processing as shown in ref 12.

4. CONCLUSION

We have explored the SRN film deposition by ICP-CVD at a low deposition temperature of 250 °C with ammonia-free gas chemistry. This is a direct deposition without the need for any postdeposition annealing. The refractive indices of these SRN films are tuned from 2.2 to 3.08 by adjusting the SiH_4:N_2 gas flow ratio during deposition. RF power also plays a part in tuning the refractive indices. The highest refractive index obtained for these SRN films is 3.08 at 1550 nm wavelength. EDS shows the presence of Si and N in different atomic % in three of these films. AFM measurements on the ~300 nm thick SRN film with n = 3.08 show an ultrasmooth surface rms roughness of 0.27 nm, which is comparable to the substrate roughness. To demonstrate its application as waveguide for photonic integration, ICP using SF_6 and CHF_3 gas chemistry was used to etch this SRN film to form a waveguide with ~90° sidewall profile. The characteristics of this direct low-temperature ICP-CVD deposited SRN film will serve as a novel platform for applications in CMOS compatible linear or nonlinear optics device applications.

AUTHOR INFORMATION

Corresponding Author

*E-mail: doris_ng@dsi.a-star.edu.sg.

Notes

The authors declare no competing financial interest.

ACKNOWLEDGMENTS

This work is a collaboration project between the Data Storage Institute and Singapore University of Technology and Design. We thank F. Tjiptoharsono for the help in sample preparation and V. Krishnamurthy for useful discussion on waveguide measurement. The fabrications were carried out in the A*STAR SERC NanoFabrication, Processing and Characterization (SnFPC) cleanroom at Data Storage Institute.

REFERENCES

(1) Jalali, B. Teaching Silicon New Tricks. *Nat. Photonics* **2007**, *1*, 193–195.
(2) Foster, M. A.; Turner, A. C.; Sharping, J. E.; Schmidt, B. S.; Lipson, M.; Gaeta, A. L. Broad-band Optical Parametric Gain on a Silicon Photonic Chip. *Nature* **2006**, *441*, 960–963.
(3) Corcoran, B.; Monat, C.; Grillet, C.; Moss, D. J.; Eggleton, B. J.; White, T. P.; O'Faolain, L.; Krauss, T. F. Green Light Emission in Silicon through Slow-light Enhanced Third-harmonic Generation in Photonic-crystal Waveguides. *Nat. Photonics* **2009**, *3*, 206–210.
(4) Foster, M. A.; Salem, R.; Geraghty, D. F.; Turner-Foster, A. C.; Lipson, M.; Gaeta, A. L. Silicon-chip-based Ultrafast Optical Oscilloscope. *Nature* **2008**, *456*, 81–85.
(5) Tan, D. T. H.; Sun, P. C.; Fainman, Y. Monolithic Nonlinear Pulse Compressor on a Silicon Chip. *Nat. Commun.* **2010**, *1*, 116.
(6) Lin, Q.; Painter, O. J.; Agrawal, G. P. Nonlinear Optical Phenomena in Silicon Waveguides: Modeling and Applications. *Opt. Express* **2007**, *15*, 16604–16644.
(7) Wang, Y.; Ng, D. K. T.; Wang, Q.; Pu, J.; Liu, C.; Ho, S. T. Low Temperature Direct Bonding of InP and Si_3N_4-coated Silicon Wafers for Photonic Device Integration. *J. Electrochem. Soc.* **2012**, *159*, H507–H510.
(8) Tan, D. T. H.; Ikeda, K.; Sun, P. C.; Fainman, Y. Group Velocity Dispersion and Self Phase Modulation in Silicon Nitride Waveguides. *Appl. Phys. Lett.* **2010**, *96*, 061101.
(9) Tom, H. W. K.; Heinz, T. F.; Shen, Y. R. Second-Harmonic Reflection from Silicon Surfaces and its Relation to Structural Symmetry. *Phys. Rev. Lett.* **1983**, *51*, 1983–1986.
(10) Sipe, J. E.; Moss, D. J.; van Driel, H. M. Phenomenological Theory of Optical Second- and Third-harmonic Generation from Cubic Centrosymmetric Crystals. *Phys. Rev. B: Condens. Matter Mater. Phys.* **1987**, *35*, 1129–1141.
(11) Shen, Y. R. Surface Properties Probed by Second-harmonic and Sum-frequency Generation. *Nature* **1989**, *337*, 519–525.
(12) Wang, T.; Ng, D. K. T.; Ng, S. K.; Toh, Y. T.; Chee, A. K. L.; Chen, G. F. R.; Wang, Q.; Tan, D. T. H. Supercontinnum Generation in Bandgap Engineered, Back-end CMOS Compatible Silicon Rich Nitride Waveguides. *Laser Photonics Rev.* **2015**, DOI: 10.1002/lpor.201500054.
(13) Kumar, A.; Taube, W. R.; Sarvanan, R.; Agarwal, P. B.; Kothari, P.; Kumar, D. Plasma Enhanced Chemical Vapor Deposited (PECVD) Silicon-Rich-Nitride Thin Films For Improving Silicon Solar Cells Efficiency. *Int. J. Sci. Eng. Technol.* **2012**, *1*, 111–116.
(14) Lipiński, M. Silicon Nitride for Photovoltaic Application. *Arch. Mater. Sci. Eng.* **2010**, *46*, 69–87.
(15) Lin, P. T.; Singh, V.; Lin, H. Y. G.; Tiwald, T.; Kimerling, L. C.; Agarwal, A. M. Low-stress Silicon Nitride Platform for Mid-infrared Broadband and Monolithically Integrated Microphotonics *Adv. Adv. Opt. Mater.* **2013**, *1*, 732–739.
(16) Mao, S. C.; Tao, S. H.; Xu, Y. L.; Sun, X. W.; Yu, M. B.; Low, G. Q.; Kwong, D. L. Low Propagation Loss SiN Optical Waveguide Prepared by Optimal Low-hydrogen Module. *Opt. Express* **2008**, *16*, 20809–20816.
(17) Olson, J. M. Analysis of LPCVD Process Conductions for the Deposition of Low Stress Silicon Nitride. Part I: Preliminary LPCVD Experiments. *Mater. Sci. Semicond. Process.* **2002**, *5*, 51–60.
(18) Ay, F.; Aydinli, A. Comparative Investigation of Hydrogen Bonding in Silicon Based PECVD Grown Dielectrics for Optical Waveguides. *Opt. Mater.* **2004**, *26*, 33–46.
(19) Martinez, F. L.; Ruiz-Merino, R.; del Prado, A.; San Andres, E.; Martil, I.; Gonzalez-Diaz, G.; Jeynes, G.; Barradas, N. P.; Wang, L.; Reehal, H. S. Bonding Structure and Hydrogen Content in Silicon Nitride Thin Films Deposited by Electron Cyclotron Resonance Plasma Method. *Thin Solid Films* **2004**, *459*, 203–207.
(20) Levy, J. S.; Gondarenko, A.; Foster, M. A.; Turner-Foster, A. C.; Gaeta, A. L.; Lipson, M. CMOS-compatible Multiple-wavelength Oscillator for On-chip Optical Interconnects. *Nat. Photonics* **2010**, *4*, 37–40.
(21) Hakki, B. W.; Paoli, T. L. CW Degradation at 300 Degrees K of GaAs Double-Heterostructure Junction Lasers 0.2. Electronic Gain. *J. Appl. Phys.* **1973**, *44*, 4113–4119.

DOI: 10.1021/acsami.5b06329
ACS Appl. Mater. Interfaces 2015, 7, 21884–21889

(22) Ferlauto, A. S.; Ferreira, G. M.; Pearce, J. M.; Wronski, C. R.; Collins, R. W.; Deng, X.; Ganguly, G. Analytical Model for the Optical Functions of Amorphous Semiconductors from the Near-infrared to Ultraviolet: Applications in Thin Film Photovoltaics. *J. Appl. Phys.* **2002**, *92*, 2424−2436.

DOI: 10.1021/acsami.5b06329
ACS Appl. Mater. Interfaces 2015, 7, 21884−21889